molecular pharmaceutics

Article

In vivo ester hydrolysis as a new approach in development of PET tracers for imaging hypoxia

Lifang Zhang, Xinyue Yao, Jianhua Cao, Haiyan Hong, Aili Zhang, Ruiyue Zhao, Yan Zhang, Zhihao Zha, Yajing Liu, Jinping Qiao, Lin Zhu, and Hank F. Kung

Mol. Pharmaceutics, **Just Accepted Manuscript** • DOI: 10.1021/acs.molpharmaceut.8b01131 • Publication Date (Web): 24 Jan 2019

Just Accepted

ACS Publications

is published by the American Chemical Society. 1155 Sixteenth Street N.W., Washington, DC 20036

In vivo ester hydrolysis as a new approach in development of PET tracers for imaging hypoxia

Lifang Zhang[a], Xinyue Yao[a], Jianhua Cao[a], Haiyan Hong[a], Aili Zhang[a], Ruiyue Zhao[a], Yan Zhang[a], Zhihao Zha[b,c], Yajing Liu[b], Jinping Qiao[a], Lin Zhu[a,b*], and Hank F Kung[b,c*]

[a] Key Laboratory of Radiopharmaceuticals, Ministry of Education, College of Chemistry, Beijing Normal University Beijing, 100875, P. R. China

[b] Beijing Institute for Brain Disorders, Capital Medical University, Beijing, 100069, P. R. China

[c] Department of Radiology, University of Pennsylvania, Philadelphia, PA 19014, USA

Corresponding author contact information**:**

Hank F. Kung, Ph.D., Department of Radiology University of Pennsylvania, 3700 Market Street, Room 305 Philadelphia, PA 19104, USA

Tel: +1 215 662 3989; Fax: +1 215 349 5035; E-mail: kunghf@gmail.com

Lin Zhu, Ph.D., Key Laboratory of Radiopharmaceuticals, Ministry of Education, College of Chemistry, Beijing Normal University, No.19, XinJieKouWai Street, Haidian District, Beijing, 100875, P.R. China

Tel: +86 10 62200772; E-mail: zhulin@bnu.edu.cn

Table of Contents

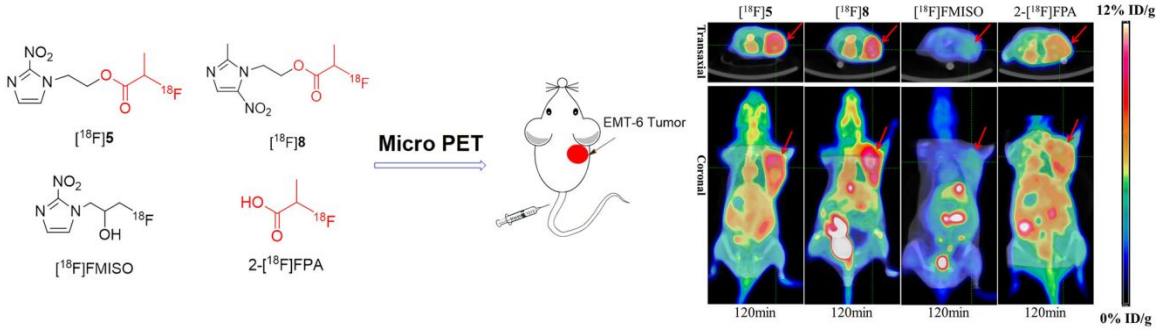

Abstract:

Hypoxia is an important biochemical and physiological condition associated with uncontrolled growth of tumor. Measurement of hypoxia in tumor tissue may be useful in characterization of tumor progression and monitoring drug treatment. [^{18}F]FMISO is the most widely employed radiotracer for imaging of hypoxic tissue with positron emission tomography (PET). However, it showed relatively low uptake in hypoxic tissues, which led to low target-to-background contrast in PET images. To overcome these shortcomings, two novel 2-fluoroproprioic acid esters, nitroimidazole derivatives, 2-fluoropropionic acid 2-(2-nitro-imidazol-1-yl)-ethyl ester (FNPFT, [^{19}F]**5**) and 2-fluoropropionic acid 2-(2-methyl-5-nitro-imidazol-1-yl)-ethyl ester (FMNPFT, [^{19}F]**8**), were prepared and tested. Radiolabeling of [^{18}F]**5** and [^{18}F]**8** were accomplished in 45 min (radiochemical purity > 95%, the decay-corrected radiochemical yield of [^{18}F]**5** was 11 ± 2%, and that of [^{18}F]**8** was 13 ± 2%, n = 5). In vitro cell uptake studies using EMT-6 tumor cells showed that both radiotracers [^{18}F]**5** and [^{18}F]**8** displayed significantly higher uptake in hypoxic cells than those under normoxic condition, while 2-[^{18}F]fluoropropionic acid (2-[^{18}F]FPA) displayed no difference. Biodistribution studies in mice bearing EMT-6 tumor showed that [^{18}F]**5**, [^{18}F]**8**, and 2-[^{18}F]FPA displayed similar tumor and major organ uptakes. Tumor uptake values for all three agents were higher than those of [^{18}F]FMISO, respectively ($P < 0.05$). This is likely due to a rapid in vivo hydrolysis of [^{18}F]**5** and [^{18}F]**8** to their metabolite, 2-[^{18}F]FPA. Micro PET imaging studies in the same

EMT-6 implanted mice tumor model also demonstrated that both [^{18}F]**5** and [^{18}F]**8** displayed similar tumor uptake comparable to that of 2-[^{18}F]FPA.

In conclusion, two new fluorine-18 labeled nitroimidazole derivatives, [^{18}F]**5** and [^{18}F]**8**, showed good tumor uptakes in mice bearing EMT-6 tumor. However, in vivo biodistribution results suggested that they were more likely reflect the predominance of in vivo produced metabolite, 2-[^{18}F]FPA, which may not be related to tumor hypoxic condition.

Keywords: Micro PET imaging; in vivo metabolism; EMT-6 tumor; nitroimidazole; hypoxia

Abbreviations

PET: Positron Emission Tomography; HPLC: High performance liquid chromatography; TLC: Thin-layer chromatography; [^{18}F]FMISO: [^{18}F]Fluoromisonidazole; [^{18}F]FAZA: [^{18}F]fluoroazomycin arabinofuranoside; [^{18}F]FETNIM: [^{18}F]fluoroerythronitroimidazole; [^{18}F]FETA: [^{18}F]fluoroetanidazole; [^{18}F]EF5: 2-(2-nitro-1*H*-imidazol-1-yl)-*N*-(2, 2, 3, 3, 3-[^{18}F]pentafluoro-propyl)acetamide; 2-[^{18}F]FPA: 2-[^{18}F]fluoropropionic acid; NITTP: 1-(2-nitro-10-imidazolyl)-2-O-tetra-hydropyranyl-3-O-toluenesulfonylpropane-diol; [^{18}F]EF3: 2-(2-nitroimidazol-1-yl)-*N*-(3, 3, 3-[^{18}F]trifluoropropyl)-acetamide; RCY:

Radiochemical yield; RCP: Radiochemical purity; OTBDMS: tert-butyldimethylsilyloxy group.

Introduction

Hypoxia in tumor tissue is an important pathological process that commonly associated with uncontrolled growth of tumor. It is considered to be a factor determining the curability of radiotherapy and chemotherapy.[1-4] The effect of hypoxia on biological processes depends on tumor type, as well as the degree and duration of oxygen deprivation.[5, 6] Thus, determining the extent of tumor hypoxia is an important factor for planning of cancer therapy.[7, 8] There is an urgent need to develop effective approaches for measuring hypoxia in tumor tissue. Currently, oxygen sensitive electrode and immunohistochemistry are gold standards for detecting hypoxic areas in tumor. However, they are not suitable for routine use due to their technical difficulty and invasiveness.[9-11] Positron emission tomography (PET) imaging may have certain advantages, which may overcome the difficulties in evaluation of hypoxia tumor tissue non-invasively. In addition, PET imaging has superior global sensitivity and quantification capability making it as one of the most promising technologies for detecting tumor hypoxia.[7, 11-13]

Originally, 2-nitroimidazole compounds, for example, [^{18}F]fluoromisonidazole ([^{18}F]FMISO, Figure 1), were developed for detecting tumor hypoxia in 1979.[14] Currently, [^{18}F]FMISO is still the most commonly used PET agent for imaging hypoxia and it is considered as a gold standard for studying hypoxia by in vivo PET imaging.[15-20] However, despite its long history and extensive literature reports, [^{18}F]FMISO has failed to gain

wide acceptance for routine clinical application. This is due to its relatively low uptake in hypoxic tumor, slow clearance from the blood and normal tissues, which contribute to low target-to-background contrast in PET images. In the past few decades, significant efforts have been reported in developing better hypoxia PET imaging agents.[12, 21-25] New nitroimidazole PET tracers with different side chains were produced and evaluated successively for PET imaging of hypoxic tumors, including the introduction of sugars ([^{18}F]fluoroazomycin arabinofuranoside, [^{18}F]FAZA),[9, 26, 27] adding hydroxyl groups ([^{18}F]fluoroerythronitroimidazole, [^{18}F]FETNIM),[28, 29] and adding amide bonds ([^{18}F]fluoroetanidazole, [^{18}F]FETA).[30, 31] (Figure 1) However, these ^{18}F-labeled 2-nitroimidazoles shared a common feature: they showed a higher hydrophilicity, thus, reduced lipophilicity for cell membrane penetration than that of [^{18}F]FMISO. These radiotracers displayed either low signal/noise ratios due to lower uptake in hypoxic lesions or slower clearance from normal tissues.[10, 11, 32] It has been shown that hydrophilicity facilitates clearance in well oxygenated tissues, while lipophilicity enhances accumulation in hypoxic tissues. In search of optimal hypoxia imaging agents achieving a delicate balance between these contrasting properties is critically important. In recent years, a new series of highly lipophilic derivatives have been studied, such as 2-(2-nitro-1*H*-imidazol-1-yl)-*N*-(2, 2, 3, 3, 3-[^{18}F]pentafluoropropyl)-acetamide ([^{18}F]EF5) and 2-(2-nitroimidazol-1-yl)-*N*-(3, 3, 3-[^{18}F]trifluoropropyl)-acetamide ([^{18}F]EF3).[33-37] (Figure 1) In addition, several hypoxia radiotracers based on

metronidazole derivatives (i.e. 5-nitroimidazole derivatives) have been reported, some of which demonstrated very favorable in vivo biodistribution properties.[38-40]

Earlier reports have pointed out that more lipophilic nitroimidazole analogs would be expected to cross cellular membranes and the blood–brain barrier (BBB) more readily and resulted in a greater initial uptake in the targeted hypoxic tissue than [^{18}F]FMISO, although there is a concomitant increase of nonspecific uptake.[21, 41, 42] This is a necessary trade-off between a higher lipophilicity (promoting cellular uptake through diffusion) and a higher liver uptake (due to a higher lipophilicity). The requirement of optimal lipophilicity leading to favorable biodistribution and pharmacokinetics of the radiotracer must be carefully balanced in the course of design an ideal hypoxia imaging agent. Recently, ^{18}F-acetyl has been conjugated to 2-nitroimidazole to form a ^{18}F-labeled fluoroacetate of 2-nitroimidazole.[43] Results of LC-MS data showed that the hypoxia tracer was hydrolyzed in vivo to hydrophilic ^{18}F-fluoroacetic acid. Results suggested that it was possible to enhance tumor uptake and speed up non-target clearance in vivo by introducing ^{18}F-aliphatic ester into nitroimidazole analogues. Additionally, previous studies reported that hydrolysable nitroimidazole aliphatic esters might be useful as radiosensitizers for cancer therapy.[44, 45] The esters were subject to enzyme-catalyzed hydrolysis in human plasma and in pure buffer solution. The length of the linear carbon chain in the aliphatic esters influences the rate of enzyme catalyzed degradation. Furthermore, studies by Johansen et al[45] also revealed large differences in chemical

stability of the nitroimidazole aliphatic ester derivatives in aqueous solution and in plasma. The hydrolysis rate of the esters was remarkably increased in human plasma, but the rate of hydrolysis was significantly decreased, or none, in buffer solution with increased length of the acyl side chain from the methyl to the pentyl. Thus, it offers flexibility to design hypoxia tracers with optimized physicochemical and pharmacokinetic characteristics using ^{18}F-labeled nitroimidazole aliphatic esters by controlling the hydrolysis rate via regulating length of the acyl side chain. This might maintain a balance between an ester acyl chain length and its hydrolysis rate, which may lead to optimal tracers for hypoxia imaging. In an attempt to control the in vivo hydrolysis and maintain the hypoxic uptake towards tumor cells envision new nitroimidazole ester derivatives may be a reasonable starting point for designing better hypoxic imaging agents.

In this work, we have developed two new nitroimidazole derivatives, 2-fluoropropionic acid 2-(2-nitro-imidazol-1-yl)-ethyl ester (FNPFT, [^{19}F]**5**), and 2-fluoropropionic acid 2-(2-methyl-5-nitro-imidazol-1-yl)-ethyl ester (FMNPFT, [^{19}F]**8**), which containing 2-fluoropropionyl ester group without changing the hypoxia-targeting nitroimidazole group. Reported herein is the synthesis of [^{18}F]NPFT ([^{18}F]**5**) and [^{18}F]MNPFT ([^{18}F]**8**) (Figure 1), and evaluation of their potentiality as hypoxia imaging agents by measuring their stability in vitro, partition coefficient, tumor cell uptake, and biodistribution/Micro PET imaging in EMT-6 tumor-bearing mice.

Experimental Section

General

Reagents and solvents

The precursor used for preparation of [^{18}F]FMISO, 1-(2-nitro-10-imidazolyl)-2-O-tetra-hydropyranyl-3-O-toluenesulfonylpropane-diol (NITTP), was purchased from Huayi Chemicals Co., Ltd. (Changshu, Jiang Su, China). Other reagents and solvents were of analytical reagent grade and purchased from commercial sources (Aldrich, Acros, or Alfa Inc.), and were used without further purification unless otherwise specified.

Instrument and consumables materials

Thin-layer chromatography (TLC) was run on pre-coated plates of silica gel 60 F254 (Merck, Darmstadt, Germany). ^{1}H NMR spectra were recorded on a 400 MHz Bruker Advance spectrophotometer (Bruker Co., Germany), ^{13}C NMR spectra were recorded on a 600 MHz JMTC-600/54/JJ (Japan Superconductor Technology, Inc., Japan), and the chemical shifts were reported as δ values (parts per million) relative to residual protons of deuterated solvent. Coupling constants are reported in Hertz (Hz). The multiplicity is defined by s (singlet), d (doublet), t (triplet), br (broad), and m (multiplet). Melting points were measured on an X-5 melting point apparatus. Mass spectrometric detection was performed in the positive ion mode on a Micromass Quattro micro API

mass spectrometer (Waters, Milford, MA) with an electrospray ionization (ESI) source and high-resolution mass spectrometry (HRMS) data was registered by an Agilent (Santa Clara, CA) G3250AA LC/MSD TOF system. Solid-phase extraction cartridges (Oasis HLB (3cc) cartridge, Sep-Pak light QMA cartridge, neutral Al_2O_3 cartridge and Sep-pak C-18 cartridge) were obtained from Waters (Milford, MA, USA). The [^{18}F]fluoride ion was produced by Peking University Cancer Hospital.

Animals

Animal studies were performed in BALB/c female mice (weight, 18 ± 2 g) bearing EMT-6 tumors (purchased from Cancer Hospital Chinese Academy of Medical Sciences, Beijing, China), which grew to right upper limb diameter of 10–15 mm. Male Sprague–Dawley rats, 6–7 weeks old, 180–220 g, were obtained from Vital River Laboratory Animal Co. Ltd (Beijing, China). All the animals were maintained according as the Chinese government guidelines for care and use of laboratory animals.

Synthesis

*1-(2-(tert-Butyldimethylsilyloxy)ethyl)-2-nitro-1H-imidazole (**2**)*

A mixture of **1** (313 mg, 2.77 mmol), (2-bromoethoxy)(tert-butyl)dimethylsi -lane (892 mg, 3.73 mmol) and potassium carbonate (K_2CO_3) (404 mg, 2.92 mmol) in 5 mL N, N-dimethylformamide (DMF) was stirred at 100°C for 4 h. The mixture was then diluted with 15 mL ethyl acetate (EtOAc) and washed by saturated solution of brine (10 mL × 3).

The organic layers were dried by anhydrous Na_2SO_4 and filtered. The filtrate was concentrated, and the residual crude product was purified by flash chromatography (EtOAc/hexane: 3/7) to give 696 mg white solid **2** (yield: 97%): ^{1}H NMR (400 MHz, $CDCl_3$) δ: 7.21 (s, 1 H), 7.20 (s, 1 H), 4.61 (t, J = 4.9 Hz, 2 H), 4.01 (t, J = 4.9 Hz, 2 H), 0.89 (s, 9 H), 0.10 (s, 6 H).

*2-(2-Nitro-1H-imidazol-1-yl)-ethanol (**3**)*

To a solution of **2** (796 mg, 2.93 mmol) in 5 mL tetrahydrofuran (THF) was added 5 mL HCl solution (0.5 mL 1% HCl in 4.5 mL ethanol) dropwise at room temperature. After 3 h, the mixture was cooled to 0°C and neutralized with 10% Na_2CO_3. The aqueous layer was extracted with dichloromethane (20 mL × 3). The organic layers were dried by anhydrous Na_2SO_4 and filtered. The filtrate was concentrated, and the residual crude product was purified by flash chromatography (EtOAc/hexane: 3/7) to give 356.4 mg yellow solid **3** (yield: 70%): ^{1}H NMR (400 MHz, DMSO) δ: 7.61 (s, 1 H), 7.16 (s, 1 H), 5.01 (t, J = 5.4 Hz, 2 H), 3.70 (t, J = 5.24 Hz, 2 H), 3.33 (s, 1 H).

*2-Fluoropropionic acid 2-(2-nitro-imidazol-1-yl)-ethyl ester ([^{19}F]**5**)*

2-Fluoropropionic acid (0.1 mL, 1.32 mmol) was dissolved in anhydrous DMF (5 mL), N,N-Diisopropylethylamine (DIPEA, 0.25 mL, 1.43 mmol), 1-Ethyl-(3-dimethylaminopropyl)carbodiimide hydrochloride (EDCl, 250 mg, 1.30 mmol), and 1-Hydroxybenzotriazole hydrate (HOBt, 180 mg, 1.33 mmol) were added under ice-water bath conditions, then dropwise with the compound **3** (105 mg, 0.67

mmol). After 2 h, the ice-water bath was removed. After stirring overnight, the mixture was diluted with 20 mL dichloromethane (DCM) and washed by saturated solution of brine (10 mL × 3). The organic layers were dried by anhydrous Na_2SO_4 and filtered. The filtrate was concentrated, and the residual crude product was purified by flash chromatography (DCM/Methanol: 100/1) to give 139 mg yellow solid [^{19}F]**5** (yield: 89.7%): Mp: 66.9–67.2°C. ^{1}H NMR (400 MHz, $CDCl_3$) δ: 7.18 (s, 1 H), 7.11 (s, 1 H), 4.90-5.08 (dq, 1 H), 4.77 (t, *J* = 5.06 Hz, 2 H), 4.60 (t, *J* = 5.04 Hz, 2 H), 1.50-1.58 (dd, 3 H). ^{13}C NMR (600 MHz, $CDCl_3$) δ: 170.04, 169.89, 128.70, 126.79, 86.18, 84.96, 63.32, 48.77, 18.39, 18.24. HRMS (ESI) calculated for $C_8H_{11}FN_3O_4$ ($M+H^+$), 232.0734; found, 232.0732.

*2-Bromo-propionic acid 2-(2-nitro-imidazol-1-yl)-ethyl ester (**4**)*

To a mixture of compound **3** (162 mg, 1.03 mmol) and triethylamine (0.4 mL, 2.88 mmol) in anhydrous DCM, bromopropionyl bromide (0.2 mL, 2.00 mmol) in anhydrous DCM (2 mL) was added dropwise in 1 h. The reaction solution was then stirred at room temperature overnight. H_2O (10 mL) was added and extracted with DCM (10 mL × 2), and the organic layers were combined and dried over anhydrous Na_2SO_4, filtered, the filtrate was evaporated and purified by flash chromatography (EtOAc/hexane: 2/3) to give product **4** (116 mg, yield: 38.7%) as a yellow oily liquid. ^{1}H NMR (400MHz, $CDCl_3$) δ: 7.19 (s, 2 H), 4.75 (t, *J* = 7.44 Hz, 2 H), 4.34 (t, *J* = 6.91 Hz, 2 H), 4.10–4.15 (m, 1 H), 1.79-1.80 (d, *J* = 6.92 Hz, 3 H). ^{13}C NMR (600 MHz, $CDCl_3$) δ: 169.81, 128.68,

127.07, 63.81, 48.85, 39.32, 21.55. HRMS (ESI) calculated for $C_8H_{11}BrN_3O_4$ ($M+H^+$), 291.9933; found, 291.9926.

*2-Fluoropropionic acid 2-(2-methyl-5-nitro-imidazol-1-yl)-ethyl ester ([^{19}F]**8**)*

Compound [^{19}F]**8** was prepared from 2-Methyl-5-nitroimidazole-1-ethanol (171 mg, 1 mmol), DIPEA (0.35 mL, 2 mmol), HOBt (270 mg, 2 mmol) and 2-fluoropropionic acid (0.15 mL, 2 mmol), with the same procedure described for compound [^{19}F]**5**. Compound [^{19}F]**8**: 146 mg yellow solid (yield: 59.6%): Mp: 71.0–71.5°C. ^{1}H NMR (400 MHz, $CDCl_3$) δ: 7.98 (s, 1 H), 4.90-5.07 (dq, 1 H), 4.66 (t, J = 5.04 Hz, 2 H), 4.55 (t, J = 3.49 Hz, 2 H), 2.54 (s, 3 H), 1.49–1.57 (dd, 3 H). ^{13}C NMR (600 MHz, $CDCl_3$) δ: 170.12, 169.97, 133.41, 86.29, 85.07, 63.71, 45.06, 18.39, 18.24, 14.45. HRMS (ESI) calculated for $C_9H_{13}FN_3O_4$ ($M+H^+$), 246.0890; found, 246.0885.

2-Bromo-propionic acid 2-(2-methyl-5-nitro-imidazol-1-yl)-ethyl ester (7)

To a mixture of 2-Methyl-5-nitroimidazole-1-ethanol (177 mg, 1.01 mmol) and triethylamine (0.4 mL, 2.88 mmol) in anhydrous DCM, bromopropionyl bromide (0.2 mL, 2.00 mmol) in anhydrous DCM (2 mL) was added dropwise in 1 h. The reaction solution was then stirred at room temperature overnight. H_2O (10 mL) was added and extracted with DCM (10 mL × 2), and the organic layers were combined and dried over anhydrous Na_2SO_4, filtered, the filtrate was evaporated and purified by flash chromatography (EtOAc/Petroleum ether: 2/1) to give product **7** (169 mg, yield: 55.4%) as a yellow oily liquid. ^{1}H NMR (400 MHz, $CDCl_3$) δ: 7.91 (s, 1 H), 4.57 (t, J = 3.12 Hz, 2 H), 4.45 (t, J

= 4.52 Hz, 2 H), 4.20–4.26 (q, 1 H), 2.50 (s, 3 H), 1.71 (d, J = 6.92 Hz, 3 H). ^{13}C NMR (600 MHz, $CDCl_3$) δ: 169.88, 151.21, 133.45, 64.09, 44.99, 39.12, 21.58, 14.72. HRMS (ESI) calculated for $C_9H_{13}BrN_3O_4$ ($M+H^+$), 306.0089; found, 306.0085.

Radiolabeling

Preparation of [^{18}F]1-(2-nitro-1-imidazolyl)-3-fluoro-2-propanol ([^{18}F]FMISO)

The aqueous solution of the [^{18}F]fluoride ion produced by the cyclotron was passed through a Sep-Pak light QMA cartridge, The cartridge was previously activated with 10 mL 1 M $NaHCO_3$ and 10 mL water, as well as dried with argon. Then the ^{18}F activity was eluted with 1.1 mL of Kryptofix 2.2.2 (K2.2.2)/K_2CO_3 solution (11.0 mg K2.2.2 and 2.0 mg K_2CO_3 in 0.93 mL acetonitrile and 0.17 mL H_2O). The eluent was then evaporated at 100°C under an argon stream. Additionally, the residue was azeotropically dried twice with 1.0 mL anhydrous acetonitrile at 100°C under an argon stream. A solution of 1 mg precursor (NITTP) in 1 mL anhydrous acetonitrile was added to the evaporation residue, and the mixture was heated at 100°C for 10 min, followed by hydrolysis with 2 M HCl (1 mL) at 100°C for 10 min. After cooling down to room temperature, 2 M NaOH (1 mL) was added to neutralize. The crude reaction mixture was subsequently delivered to a neutral Al_2O_3 cartridge and a Sep-pak C-18 cartridge for purification. [^{18}F]FMISO was trapped on the cartridge and eluted with 1 mL ethanol. The pure product was diluted with saline to 10% ethanol solution, and then sterilized by

passing through a 0.22 μm sterile membrane. The structure of the purified product was confirmed by HPLC with a gamma ray radio-detector and a UV detector at 320 nm, as well as the radiochemical purity (RCP). The HPLC condition was as follow: Phenomenex Gemini C18 (4.6 mm × 250 mm, 5 μm), mobile phase: acetonitrile/H_2O 3/7 (V/V), 1 mL/min. The RCP was also measured by Radio-TLC, with a mobile phase acetonitrile/H_2O 85/15.

*Preparation of [^{18}F]**5** and [^{18}F]**8***

[^{18}F]KF/18-crown-6 complex was prepared as previously described for [^{18}F]FMISO. A solution of precursor **4** (2 mg) or precursor **7** (2 mg) in 1 mL acetonitrile was added to the dried [^{18}F]KF/18-crown-6 complex and heated at 80°C for 10 min. After cooling down to room temperature, the reaction mixture was quickly diluted with 5 mL buffer solution (pH = 6.40) containing 0.2 M disodium hydrogen phosphate and 0.1 M citric acid, and subsequently passed through an Oasis HLB cartridge. The cartridge was rinsed with 2 mL 10% ethanol/H_2O (V/V) and then eluted with 1 mL ethanol to obtain [^{18}F]**5** or [^{18}F]**8**. The pure product was diluted with saline to 10% ethanol solution, and then sterilized by passing through a 0.22 μm sterile membrane. The structure and RCP of the product was confirmed by HPLC with a gamma ray radio-detector and a UV detector at 320 nm. The HPLC condition was as follow: Column was Phenomenex Gemini C18 (4.6 mm × 250 mm, 5 μm), mobile phase: 0.1% Formic acid solution(A), acetonitrile (B), 1 mL/min with a gradient as shown below: from 0 to 3 min, A 99%, B 1%; from 3 to 10

min, gradient A 99-5%, B 1-95%; from 10 to 15 min, gradient A 5-80%, B 95-20%; from 15 to 18 min, gradient A 80-99%, B 20-1%. The RCP was also measured by Radio-TLC, with a mobile phase CH_2Cl_2/CH_3OH = 9/1.

Preparation of 2-[^{18}F]FPA

2-[^{18}F]FPA was prepared according to the method previously described.[46]

In vitro stability study

The in vitro stability of [^{18}F]**5** and [^{18}F]**8** were examined by incubating in 1 mL saline for 2 h at room temperature, and the RCP was measured by Radio-TLC and Radio-HPLC using chromatographic conditions as previously described.

In vitro metabolism studies in rat serum

Rat blood was freshly drawn from an anesthetized SD rat into tubes. Centrifugation was performed at 5000 g for 5 min, and the supernatant was taken as rat serum. Incubations were carried out at 37 °C in a water bath. The hydrolysis reactions were initiated by adding [^{18}F]**5** or [^{18}F]**8** (~3 MBq), in 100 μL 10% ethanol solution to preheated blood samples (900 μL) or 10% ethanol solution (as control). Aliquots (100 μL) were taken from blood at 2, 5 and 10 min and were deproteinized by mixing with acetonitrile (200 μL). After centrifuging for 5 min at 14,000 rpm, 10 μL of the supernatant layer was analyzed by analytical HPLC using Phenomenex Gemini C18 column (4.6 mm × 250 mm, 5 μm) with mobile phase consistent of 20 mM NaH_2PO_4 (A)

and acetonitrile (B), a flow rate of 1 mL/min with a gradient as shown below: from 0 to 3 min, A 99%, B 1%; from 3 to 10 min, gradient A 99-5%, B 1-95%; from 10 to 15 min, gradient A 5-80%, B 95-20%; from 15 to 18 min, gradient A 80-99%, B 20-1%.

Determination of the partition coefficient (log P)

Log *P* was assessed by mixing radiotracer [^{18}F]**5**, [^{18}F]**8** or [^{18}F]FMISO with 1-octanol and phosphate buffer (0.1 M, pH 7.4) system in a centrifuge tube. The tube was shaken uniformity on a Vortex oscillator (Vortex-Genie 2) for 3 min and then centrifuged at 5000 g for 5 min. Three samples (0.2 mL each) from the 1-octanol and buffer layers were then measured for radioactivity. The partition coefficient was calculated as the mean value of counts per minute in 1-octanol divided by that of the buffer. The measurement was performed for three times, and the final partition coefficient value was expressed as log *P*.

In vitro cell uptake

Cell uptake studies were evaluated using the murine mammary carcinoma cells EMT6 cell lines, which were purchased from Cancer Hospital Chinese Academy of Medical Sciences, Beijing, China. The cell was maintained (5% CO_2 incubator at 37°C) in RPMI 1640 medium (purchased from Corning) containing 10% fetal bovine serum and 1% antibiotics mixture. The cells were dispersed in 20 mL fresh RPMI medium to achieve final concentration of approximately 2×10^6 cells/mL. Aliquots of 10 mL were

added into glass vials and incubated at 37°C with gentle magnetic stirring under normoxic (5% CO_2 plus 95% air) or hypoxic (5% CO_2 plus 95% N_2) atmosphere. In addition, the cells were equilibrated for 60 min in either normoxic or hypoxic conditions, then the radiotracer ([^{18}F]FMISO, 2-[^{18}F]FPA, [^{18}F]**5** or [^{18}F]**8**, 0.37 MBq/100 μL) was added to each glass vial and incubated for 30, 60, 120 and 240 min. 1 mL samples were removed at each time point. From the samples, four aliquots (200 μL) were centrifuged at 1500 rpm for 5 min to separate the cells from the supernatant. 90 μL of the supernatant was removed for counting as A, and 110 μL of residue medium containing cells was counted as B. The cell uptake was calculated as $C_{in}/C_{out}/10^6$ cells (the uptake in 10^6 cells), C_{in}/C_{out} = (B – A)/A. The cell viability was detected by trypan blue exclusion assay during the whole procedure, and the viability of cells was more than 90%. Statistical analysis was performed using the Student's *t*-test (n = 3 at each time point).

Biodistribution studies

Biodistribution studies were assessed in BALB/c female mice bearing EMT-6 tumor. 0.1 mL of radiotracer ([^{18}F]**5** or [^{18}F]**8**, ~1.11 MBq) was intravenously injected into each mouse. Five mice for each time were sacrificed at 30, 90, and 120 min post-injection. The organs or tissues (blood, brain, heart, lung, liver, spleen, kidney, stomach, bone, muscle, skin, and tumor) were collected, weighed and the corresponding radio-activities were assayed with a gamma counter. The results were expressed as the

percent uptake of injected dose per gram of tissue (%ID/g) and presented as mean ± SD. [^{18}F]FMISO and 2-[^{18}F]FPA were evaluated in the same animal model and used for comparison.

Micro PET/CT imaging

PET imaging was performed on a Micro PET/CT scanner (Siemens Invenon MM) using BALB/c female mice bearing EMT-6 tumor. [^{18}F]**5**, [^{18}F]**8**, [^{18}F]FMISO or 2-[^{18}F]FPA (5.55–11.1 MBq/0.1 mL) was intravenously administered to mice via tail vein. At 30, 60, 90 and 120 min post injection, mice were anesthetized with 2% isoflurane inhalation, and fixed on the machine in a prone position. At each time point, static imaging was obtained with 5 min CT scanning followed by 10 min PET. PET/CT Image was reconstructed with OSEM3D. Image analysis was carried out using Invenon Research Workplace software.

Statistical Analysis

Data were presented as mean ± standard deviation (SD). All statistical tests were conducted using the IBM SPSS Statistics Version 20.0 for Windows (SPSS, Inc, IBM Company). The independent samples nonparametric test was used to compare the difference of 2 quantitative groups. Pearson product-moment correlation coefficient (r) was used for correlation analysis between continuous variables. A P value of less than 0.05 was considered statistically significant.

Results and discussion

Synthesis

The radiolabeling precursor **4** and non-radioactive standard [^{19}F]**5** were prepared by reactions shown in the **Scheme 1**. Starting material **2** was synthesized by N-alkylation of commercially available 2-nitroimidazole. The protecting group OTBDMS of compound **2** was removed by treating with 1% HCl to obtain **3**. The acylation of compound **3** with bromopropionyl bromide and 2-flupropionic acid, respectively, produced the radiolabeling precursor **4** and non-radioactive standard [^{19}F]**5**. The radiolabeling precursor **7** and non-radioactive standard [^{19}F]**8** were prepared by reactions shown in the **Scheme 2**. Starting material **6** was purchased directly from commercial sources. The acylation of compound **6** with 2-bromopropionyl bromide and 2-flupropionic acid, respectively, produced the radiolabeling precursor **7** and non-radioactive standard [^{19}F]**8**. These procedures yielded the desired products after chromatographic isolation. All compounds were characterized by ^{1}H NMR, ^{13}C NMR and HRMS (Compound **2** and **3** were synthesized according to the previously reported methods,[43] only ^{1}H NMR data were included). Results were consistent with proposed structures.

Radiolabeling

Preparation of [^{18}F]FMISO

The radiosynthesis of [^{18}F]FMISO was carried out according to the previously reported methods.[23, 40] [^{18}F]FMISO was synthesized from the precursor NITTP by a nucleophilic substitution fluorination reaction followed by acid hydrolysis of alcohol protecting group. The pure radiotracer of [^{18}F]FMISO was obtained by using a neutral Al_2O_3 cartridge and a Sep-pak C-18 cartridge. The decay-corrected radiochemical yield of [^{18}F]FMISO was 25 ± 5% (n = 5). The preparation took about 60 min. Radio-HPLC and radio-TLC analysis showed that the RCP of [^{18}F]FMISO was more than 95%. The radiochemical identity was confirmed by HPLC (see Supporting information, Figure S1) ([^{18}F]FMISO = 3.9 min, [^{19}F]FMISO = 3.8 min).

*Preparation of [^{18}F]**5** and [^{18}F]**8***

[^{18}F]**5** and [^{18}F]**8** were synthesized from the corresponding bromo precursors **4** and **7** by the reactions shown in **Scheme 3**. The bromo precursors, **4** and **7**, were reacted with dried [^{18}F]KF/18-crown-6 complex in acetonitrile at 80°C for 10 min. The radiotracers were purified with Oasis HLB cartridge and reformulated in 10% ethanol/saline. The decay-corrected radiochemical yields of [^{18}F]**5** was 11 ± 2% (n = 5), and [^{18}F]**8** was 13 ± 2% (n = 5). The synthesis time was about 45 min. Radio-HPLC and radio-TLC analysis showed that the RCP of [^{18}F]**1** and [^{18}F]**2** were more than 95%. The specific activity of [^{18}F]**5** and [^{18}F]**8** were 30 ± 2 GBq/μmol (n = 5) and 61 ± 8 GBq/μmol (n = 5), respectively. The radiochemical identity was confirmed by HPLC (Supporting information Figure S2 and Figure S3). ([^{18}F]**5** = 13.5 min, [^{19}F]**5** = 13.4 min; [^{18}F]**8** =

13.6 min, [^{19}F]**8** = 13.4 min).

Preparation of 2-[^{18}F]FPA

The radiosynthesis of 2-[^{18}F]FPA was carried out according to the previously reported methods. The decay-corrected radiochemical yields of 2-[^{18}F]FPA was 37 ± 10% (n = 5). The synthesis time was about 60 min. Radio-HPLC analysis showed that the RCP of 2-[^{18}F]FPA was more than 95%.

Determination of the partition coefficient (log P)

The partition coefficient (between octanol and 0.1 M phosphate buffer, pH 7.4) was conducted by the method described in experimental section. The log *P* was calculated shown in Table 1. The log *P* of [^{18}F]**5** and [^{18}F]**8** were 0.42 and 0.63, comparable to that of [^{18}F]FMISO (0.38). The values for all three agents were statistically similar.

In vitro stability study

After incubating with saline up to 2 h after preparation, the radiochemical purities of [^{18}F]**5** and [^{18}F]**8** were over 95% suggesting their great stability in vitro for further investigation. These two tracers displayed excellent in vitro stability in saline.

In vitro metabolism studies

In vitro stability of these two tracers, [^{18}F]**5** and [^{18}F]**8**, were evaluated in the presence of rat serum. The key difference between saline and rat serum is that in rat

blood the tracers were exposed to various enzymes which might hydrolyze the ester linkage. Measurement of potential radioactive metabolites and the rate of hydrolysis kinetics were carried out after incubating the samples in rat blood at 37°C. The percentages of unchanged [^{18}F]**5** and [^{18}F]**8** at different time points was shown in Table 2. The percentage of intact parent compound [^{18}F]**5** was 9.4% after incubating in rat blood for 2 min, while [^{18}F]**8** was 15.2%. After incubating for 10 min, both radiotracers [^{18}F]**5** and [^{18}F]**8** were very closed to completely hydrolyzed. Furthermore, the radiolabeled metabolite was more polar than the original parent radiotracers, which was likely the expected product, 2-[^{18}F]FPA, after the cleavage of the ester bond. (See Supporting information Figure S4, Figure S5 and Figure S6**)**

Results of in vitro hydrolysis of [^{18}F]**5** and [^{18}F]**8** indicated that the rate of hydrolysis of [^{18}F]**5** was faster than that [^{18}F]**8** in rat blood. Due to the existence of ester groups in the radiotracers, it would be reasonable to suspect that esterases in the blood might catalyze the hydrolysis of these two tracers. After the hydrolysis 2-[^{18}F]FPA was expected to be the major labeled compound in the circulating blood. It was known that 2-[^{18}F]FPA also showed high tumor uptake in tumor models.[46] Therefore, 2-[^{18}F]FPA might be a major contributor to the observed uptake in EMT-6 tumor tissue in vivo.

In vitro cell uptake

In vitro cellular uptake of [^{18}F]**5**, [^{18}F]**8**, [^{18}F]FMISO and 2-[^{18}F]FPA (Figure 2A,

2B, 2C and 2D, respectively) in EMT-6 cells under hypoxic and normoxic conditions were determined according to previous reported methods.[47-49] This method of in vitro study has been successfully validated in our laboratory in the evaluation of PEG-modified nitroimidazole derivatives.[50] [^{18}F]FMISO was used as a gold standard for comparison, while 2-[^{18}F]FPA as a negative control. As expected, [^{18}F]FMISO (Figure 2C) showed a significantly greater accumulation in EMT-6 cells after 1 h in hypoxic conditions ($P < 0.01$), while the uptakes of 2-[^{18}F]FPA (Figure 2D) displayed no difference between hypoxic cells and normoxic cells ($P > 0.05$). Under similar hypoxia conditions, cell uptakes of [^{18}F]**5** and [^{18}F]**8** (Figure. 2A and 2B, respectively) showed initial increase and follow by a small reduction at 2 h. Similar to that of [^{18}F]FMISO, both [^{18}F]**5** and [^{18}F]**8** showed significantly higher ($P < 0.05$) cellular uptakes under the hypoxia condition than that under the normoxic condition at all time points. In contrast, 2-[^{18}F]FPA (Figure. 2D) displayed no difference between hypoxic and normoxic conditions. Results in Figure 2 both two new radiotracers displayed highly significant hypoxia selectivity in EMT-6 cells.

Biodistribution studies

Biodistribution of [^{18}F]**5**, [^{18}F]**8**, [^{18}F]FMISO as well as 2-[^{18}F]FPA were evaluated in BALB/c mice implanted with EMT-6 tumor, which was commonly used as hypoxia tumor model.[51-53] Results of biodistribution expressed as the percentage injected dose per

gram tissue (%ID/g) for tissues of various organs of mice were presented in Tables 3. Biodistribution study showed that [^{18}F]**5** and [^{18}F]**8** displayed a high uptake (%ID/g, n = 5) in all major organs (Table 3A, 3B and 3C). Specifically, the tumor uptakes of [^{18}F]**5** were 8.49 ± 0.72, 8.89 ± 0.42 and 8.69 ± 0.78 %ID/g at 30, 60 and 120 min post-injection, while [^{18}F]**8** were 8.71 ± 0.81, 9.03 ± 1.21, 8.41 ± 0.93 %ID/g. Comparable tumor uptake values were also observed for 2-[^{18}F]FPA (tumor uptake was 8.61 ± 0.33, 8.52 ±0.51 and 7.95 ± 0.37 %ID/g at 30, 60 and 120 min post-injection. All three agents, [^{18}F]**5** and [^{18}F]**8** and 2-[^{18}F]FPA showed similar uptake in all major organs and the uptakes at 30, 60 and 120 min were remarkably similar. Lipophilicity (Table 1) appeared not to play a role in tumor uptake. Since in vitro studies in the presence of blood showed that [^{18}F]**5** and [^{18}F]**8** decomposed to 2-[^{18}F]FPA vis esterase hydrolysis, similar results of biodistribution for these three agents suggested that the biodistribution in vivo might be predominantly determined by the 2-[^{18}F]FPA. The tumor uptake for [^{18}F]FMISO was 4.41 ± 0.83, 5.43 ± 0.62 and 3.24 ± 1.58 %ID/g at 30, 60 and 120 min, respectively, using the same mice tumor model. Similar to the results above, at all three time points the tumor uptakes showed no change. The tumor uptake for [^{18}F]**5** and [^{18}F]**8** and 2-[^{18}F]FPA showed noticeable higher tumor uptake (7.9 to 9.0 %ID/g) at all three time points than those for [^{18}F]FMISO (4.4 to 3.2 %ID/g) ($P < 0.05$); however, the blood levels for [^{18}F]**5** and [^{18}F]**8** and 2-[^{18}F]FPA were also higher leading to lower tumor to blood ration when compared to that of [^{18}F]FMISO. Faster in vivo kinetics of [^{18}F]FMISO also led to lower

uptake in retention in all major organs. However, it is likely that the in vivo biodistribution of [^{18}F]**5** and [^{18}F]**8** was determined by a rapid in vivo hydrolysis to possible metabolite, 2-[^{18}F]FPA; therefore, the higher and selective hypoxic cell uptake measured by in vitro cell uptake studies (Figure 2) were not observed in the in vivo biodistribution study in EMT-6 mice model.

Micro PET/CT imaging

Using the same EMT-6 tumor-bearing mice micro PET images were acquired at 30, 60, 90, 120 min post-injection of [^{18}F]**5**, [^{18}F]**8**, 2-[^{18}F]FPA and [^{18}F]FMISO, respectively (Figure 3 and 4). PET images demonstrated that the EMT-6 tumors were clearly visualized using either [^{18}F]**5** or [^{18}F]**8**, and the tumor uptakes for [^{18}F]**5**, [^{18}F]**8** and 2-[^{18}F]FPA were very comparable at 120 min post-injection (Figure 4). While [^{18}F]FMISO displayed a lower tumor uptake and less uptake in all other major organs. This is similar to the results of biodistribution study measured by dissection method.

Although results of higher tumor uptake in the PET images of [^{18}F]**5** and [^{18}F]**8**, the tumors looked very distinctive (Figure 4); however, the tumor uptake observed appeared to be associated with the metabolite, 2-[^{18}F]FPA, which was likely a major contributor in tumor uptake. Additional studies will be needed to see how much of the original imidazole derivatives, if any, have contributed to the in vivo hypoxia tumor uptake observed in the EMT-6 tumor model. The ester linkage may not be a useful linker

for 2-[^{18}F]FPA in developing novel hypoxic targeting agents.

It has been reported that 2-[^{18}F]FPA [46] accumulated in prostate cancers with high tumor to background ratios, and it may be useful in the clinical diagnosis of prostate cancer in humans. In general, ^{18}F labeled fluoro-alkyl fatty acids[54] displayed tumor uptakes. The mechanism(s) of uptake and their relationship with hypoxia conditions has not been reported. Although, 2-[^{18}F]FPA did not showed preference for in vitro tumor cell uptake under hypoxia condition (Figure 2D). There is a hard lesson to be learned that in vivo metabolism of these nitroimidazole ester derivatives, instead of the tumor hypoxia condition, may be the driving force determining the outcome of in vivo biodistribution.

Conclusions

In summary, two new 2-fluoroproprionic acid esters of nitroimidazole, 2-fluoropropionic acid 2-(2-nitro-imidazol-1-yl) ethyl ester, **5** and 2-fluoropropionic acid 2-(2-methyl-5-nitro-imidazol-1-yl) ethyl ester, **8** ([^{18}F]**5** and [^{18}F]**8**) have been synthesized and evaluated as specific PET tracers for hypoxia imaging. In vivo biodistribution results suggested that they were more likely reflecting predominance of in vivo produced metabolite, 2-[^{18}F]FPA, which formed after an iv injection.

Acknowledgment

This work was supported in part by grants from the National Key Research and Development Program of China (2016YFC1306300) and Beijing Municipal Science & Technology Commission (Z151100003915116).

Supporting Information

Supporting Information describing the HPLC profiles of [^{18}F]FMISO, [^{18}F]**5** and [^{18}F]**8** for this paper is available in a separate file.

References:

1. Wilson, W. R.; Hay, M. P. Targeting hypoxia in cancer therapy. *Nat. Rev. Cancer.* **2011,** *11*, (6), 393-410.
2. Vaupel, P.; Mayer, A. Hypoxia in cancer: significance and impact on clinical outcome. *Cancer. Metastasis. Rev.* **2007,** *26*, (2), 225-239.
3. Tamaki, N.; Hirata, K. Tumor hypoxia: a new PET imaging biomarker in clinical oncology. *Int. J. Clin. Oncol.* **2016,** *21*, (4), 619-625.
4. Grimes, D. R.; Warren, D. R.; Warren, S.; Grimes, D. R.; Warren, S. Hypoxia imaging and radiotherapy: bridging the resolution gap. *Br. J. Radiol.* **2017,** *90*, (1076), 20160939.
5. Yip, C.; Blower, P. J.; Goh, V.; Landau, D. B.; Cook, G. J. R. Molecular imaging of hypoxia in non-small-cell lung cancer. *Eur. J. Nucl. Med. Mol. Imaging.* **2015,** *42*, (6), 956-976.
6. Bristow, R. G.; Hill, R. P. Hypoxia and metabolism. Hypoxia, DNA repair and genetic instability. *Nat. Rev. Cancer.* **2008,** *8*, (3), 180-192.
7. Stieb, S.; Guckenberger, M.; Riesterer, O.; Stieb, S.; Eleftheriou, A.; Warnock, G.; Warnock, G. Longitudinal PET imaging of tumor hypoxia during the course of radiotherapy. *Eur. J. Nucl. Med. Mol. Imaging.* **2018**, (Suppl 5), 1-17.
8. Horsman, M. R.; Mortensen, L. S.; Petersen, J. B.; Busk, M.; Overgaard, J. Imaging hypoxia to improve radiotherapy outcome. *Nat. Rev. Clin. Oncol.* **2012,** *9*, (12), 674-687.
9. Savi, A.; Incerti, E.; Fallanca, F.; Bettinardi, V.; Compierchio, A.; Gianolli, L.; Picchio, M.; Rossetti, F.; Negri, G.; Zannini, P.; Monterisi, C. First evaluation of PET-based human biodistribution and dosimetry of (^{18})F-FAZA, a tracer for imaging tumor hypoxia. *J. Nucl. Med.* **2017,** *58*, (8), 1224-1229.
10. Peeters, S. G.; Zegers, C. M.; Yaromina, A.; Van, E. W.; Dubois, L.; Lambin, P. Current preclinical and clinical applications of hypoxia PET imaging using 2-nitroimidazoles. *Q. J. Nucl. Med. Mol. Imaging.* **2015,** *59*, (1), 39-57.
11. Fleming, I. N.; Manavaki, R.; Blower, P. J.; Baldry, C.; West, C.; Williams, K. J.; Harris, A. L.; Lord, S.; Domarkas, J.; Gilbert, F. J. Imaging tumour hypoxia with positron emission tomography. *Br. J. Cancer.* **2015,** *112*, (2), 238-250.
12. Lopci, E.; Grassi, I.; Chiti, A.; Nanni, C.; Cicoria, G.; Toschi, L.; Fonti, C.; Lodi, F.; Mattioli, S.; Fanti, S. PET radiopharmaceuticals for imaging of tumor hypoxia: a review of the evidence. *Am. J. Nucl. Med. Mol. Imaging.* **2014,** *4*, (4), 365-384.
13. Farwell, M. D.; Pryma, D. A.; Mankoff, D. A. PET/CT imaging in cancer: Current applications and future directions. *Cancer.* **2014,** *120*, (22), 3433-3445.

14. Chapman, J. D. Hypoxic sensitizers--implications for radiation therapy. *N. Engl. J. Med.* **1979,** *301*, (26), 1429-1432.

15. Rasey, J. S.; Koh, W. J.; Grierson, J. R.; Grunbaum, Z.; Krohn, K. A. Radiolabelled fluoromisonidazole as an imaging agent for tumor hypoxia. *Int. J. Radiat. Oncol. Biol. Phys.* **1989,** *17*, (5), 985-991.

16. Cheng, J.; Lei, L.; Xu, J.; Sun, Y.; Zhang, Y.; Wang, X.; Pan, L.; Shao, Z.; Zhang, Y.; Liu, G. ^{18}F-fluoromisonidazole PET/CT: a potential tool for predicting primary endocrine therapy resistance in breast cancer. *J. Nucl. Med.* **2013,** *54*, (3), 333-340.

17. Kobayashi, H.; Hirata, K.; Yamaguchi, S.; Terasaka, S.; Shiga, T.; Houkin, K. Usefulness of FMISO-PET for glioma analysis. *Neurol. Med. Chir.* **2013,** *53*, (11), 773-778.

18. Rajendran, J. G.; Krohn, K. A. F-18 fluoromisonidazole for imaging tumor hypoxia: imaging the microenvironment for personalized cancer therapy. *Semin. Nucl. Med.* **2015,** *45*, (2), 151-162.

19. Bekaert, L.; Valable, S.; Lechapt-Zalcman, E.; Ponte, K.; Collet, S.; Constans, J.-M.; Levallet, G.; Bordji, K.; Petit, E.; Branger, P.; Emery, E.; Manrique, A.; Barre, L.; Bernaudin, M.; Guillamo, J.-S. [^{18}F]-FMISO PET study of hypoxia in gliomas before surgery: correlation with molecular markers of hypoxia and angiogenesis. *Eur. J. Nucl. Med. Mol. Imaging.* **2017,** *44*, (8), 1383-1392.

20. Li, H.; Xu, D.; Zhang, X.; Mi, Y.; Dong, M.; Lin, Y.; Wang, B.; Li, G.; Han, X.; Ruan, Q.; Guo, S. Dosimetry study of (^{18})F-FMISO + PET/CT hypoxia imaging guidance on intensity-modulated radiation therapy for non-small cell lung cancer. *Clin. Transl. Oncol.* **2018,** *20*, (10), 1329-1336.

21. Nunn, A.; Linder, K.; Strauss, H. W. Nitroimidazoles and imaging hypoxia. *Eur. J. Nucl. Med.* **1995,** *22*, (3), 265-280.

22. Ballinger, J. R. Imaging hypoxia in tumors. *Semin. Nucl. Med.* **2001,** *31*, (4), 321-329.

23. Kurihara, H.; Honda, N.; Kono, Y.; Arai, Y. Radiolabelled agents for PET imaging of tumor hypoxia. *Curr. Med. Chem.* **2012,** *19*, (20), 3282-3289.

24. Cabral, P.; Cerecetto, H. Radiopharmaceuticals in tumor hypoxia imaging: a review focused on medicinal chemistry aspects. *Anticancer. Agents. Med. Chem.* **2017,** *17*, (3), 318-332.

25. Bonnitcha, P.; Grieve, S.; Figtree, G. Clinical imaging of hypoxia: Current status and future directions. *Free. Radical. Biol. Med.* **2018,** *126*, 296-312.

26. Sorger, D.; Patt, M.; Kumar, P.; Wiebe, L. I.; Barthel, H.; Seese, A.; Dannenberg, C.; Tannapfel, A.; Kluge, R.; Sabri, O. [^{18}F]Fluoroazomycinarabinofuranoside (^{18}FAZA) and [^{18}F]Fluoromisonidazole (^{18}FMISO): a comparative study of their selective uptake in hypoxic cells and PET imaging in experimental rat tumors. *Nucl. Med. Biol.* **2003,** *30*, (3), 317-326.

27. Melsens, E.; Ceelen, W.; Pattyn, P.; De, V. E.; De, W. O.; De, V. E.; De, W. O.; Ceelen, W.; Pattyn, P.; Descamps, B.; Vanhove, C.; Kersemans, K.; Goethals, I.; Brans, B.; De, V. F. Hypoxia imaging with (^{18})F-FAZA PET/CT predicts radiotherapy response in esophageal adenocarcinoma xenografts. *Radiat. Oncol.* **2018,** *13*, (1), 39.

28. Yang, D. J.; Wallace, S.; Cherif, A.; Li, C.; Gretzer, M. B.; Kim, E. E.; Podoloff, D. A. Development of F-18-labeled fluoroerythronitroimidazole as a PET agent for imaging tumor hypoxia. *Radiology.* **1995,** *194*, (3), 795-800.

29. Gronroos, T.; Eskola, O.; Lehtio, K.; Minn, H.; Marjamaki, P.; Bergman, J.; Haaparanta, M.; Forsback, S.; Solin, O. Pharmacokinetics of [^{18}F]FETNIM: a potential marker for PET. *J. Nucl. Med.* **2001,** *42*, (9), 1397-1404.

30. Tewson, T. J. Synthesis of [^{18}F]fluoroetanidazole: a potential new tracer for imaging hypoxia. *Nucl. Med. Biol.* **1997,** *24*, (8), 755-760.

31. Barthel, H.; Wilson, H.; Collingridge, D. R.; Brown, G.; Osman, S.; Luthra, S. K.; Brady, F.; Workman, P.; Price, P. M.; Aboagye, E. O. In vivo evaluation of [^{18}F]fluoroetanidazole as a new marker for imaging tumour hypoxia with positron emission tomography. *Br. J. Cancer.* **2004,** *90*, (11), 2232-2242.

32. Minn, H.; Gronroos, T. J.; Komar, G.; Eskola, O.; Lehtio, K.; Tuomela, J.; Seppanen, M.; Solin, O. Imaging of tumor hypoxia to predict treatment sensitivity. *Curr. Pharm. Des.* **2008,** *14*, (28), 2932-2942.

33. Komar, G.; Seppanen, M.; Eskola, O.; Lindholm, P.; Gronroos, T. J.; Forsback, S.; Sipila, H.; Evans, S. M.; Solin, O.; Minn, H. ^{18}F-EF5: a new PET tracer for imaging hypoxia in head and neck cancer. *J. Nucl. Med.* **2008,** *49*, (12), 1944-1951.

34. Koch, C. J.; Scheuermann, J. S.; Divgi, C.; Judy, K. D.; Kachur, A. V.; Freifelder, R.; Reddin, J. S.; Karp, J.; Stubbs, J. B.; Hahn, S. M.; Driesbaugh, J.; Smith, D.; Prendergast, S.; Evans, S. M. Biodistribution and dosimetry of ^{18}F-EF5 in cancer patients with preliminary comparison of ^{18}F-EF5 uptake versus EF5 binding in human glioblastoma. *Eur. J. Nucl. Med. Mol. Imaging.* **2010,** *37*, (11), 2048-2059.

35. Chitneni, S. K.; Bida, G. T.; Zalutsky, M. R.; Dewhirst, M. W. Comparison of the hypoxia PET tracer ^{18}F-EF5 to immunohistochemical marker EF5 in 3 different human tumor xenograft models. *J. Nucl. Med.* **2014,** *55*, (7), 1192-1197.

36. Silvoniemi, A.; Laitinen, T.; Forsback, S.; Saunavaara, V.; Solin, O.; Gronroos, T. J.; Minn, H.; Silvoniemi, A.; Suilamo, S.; Gronroos, T. J.; Minn, H.; Suilamo, S.; Saunavaara, V.; Loyttyniemi, E.; Vaittinen, S. Repeatability of tumour hypoxia imaging using [(^{18})F]EF5 PET/CT in head and neck cancer. *Eur. J. Nucl. Med. Mol. Imaging.* **2018,** *45*, (2), 161-169.

37. Mahy, P.; De Bast, M.; de Groot, T.; Cheguillaume, A.; Gillart, J.; Haustermans, K.; Labar, D.; Gregoire, V. Comparative pharmacokinetics, biodistribution, metabolism and hypoxia-dependent uptake of [^{18}F]-EF3 and [^{18}F]-MISO in rodent tumor models. *Radiother. Oncol.* **2008,** *89*, (3), 353-360.

38. Yang, D. J.; Ilgan, S.; Higuchi, T.; Zareneyrizi, F.; Oh, C. S.; Liu, C. W.; Kim, E. E.; Podoloff, D. A. Noninvasive assessment of tumor hypoxia with ^{99m}Tc labeled metronidazole. *Pharm. Res.* **1999,** *16*, (5), 743-750.

39. Ito, M.; Yang, D. J.; Mawlawi, O.; Mendez, R.; Oh, C. S.; Azhdarinia, A.; Greenwell, A. C.; Yu, D. F.; Kim, E. E. PET and planar imaging of tumor hypoxia with labeled metronidazole. *Acad. Radiol.* **2006,** *13*, (5), 598-609.

40. Bejot, R.; Carroll, L.; Bhakoo, K.; Declerck, J.; Gouverneur, V. A fluorous and click approach for screening potential PET probes: Evaluation of potential hypoxia biomarkers. *Bioorg. Med. Chem.* **2012,** *20*, (1), 324-329.

41. Yamamoto, F.; Oka, H.; Antoku, S.; Ichiya, Y.-I.; Masuda, K.; Maeda, M. Synthesis and characterization of lipophilic 1-[^{18}F]Fluoroalkyl-2-nitroimidazoles for imaging hypoxia. *Biol. Pharm. Bull.* **1999,** *22*, (6), 590-597.

42. Yamamoto, F.; Aoki, M.; Furusawa, Y.; Ando, K.; Kuwabara, Y.; Masuda, K.; Sasaki, S.; Maeda, M. Synthesis and evaluation of 4-bromo-1-(3-[^{18}F]fluoropropyl)-2-nitroimidazole with a low energy LUMO orbital designed as brain hypoxia-targeting imaging agent. *Biol. Pharm. Bull.* **2002,** *25*, (5), 616-621.

43. Zha, Z.; Zhu, L.; Liu, Y.; Du, F.; Gan, H.; Qiao, J.; Kung, H. F. Synthesis and evaluation of two novel 2-nitroimidazole derivatives as potential PET radioligands for tumor imaging. *Nucl. Med. Biol.* **2011,** *38*, (4), 501-508.

44. Johansen, M.; Mollgaard, B.; Wotton, P. K.; Larsen, C.; Hoelgaard, A. In vitro evaluation of dermal prodrug delivery - transport and bioconversion of a series of aliphatic esters of metronidazole. *Int. J. Pharm.* **1986,** *32*, (2), 199-206.

45. Johansen, M.; Larsen, C. A comparison of the chemical stability and the enzymic hydrolysis of a series of aliphatic and aromatic ester derivatives of metronidazole. *Int. J. Pharm.* **1985,** *26*, (3), 227-241.

46. Pillarsetty, N. V.; Punzalan, B.; Larson, S. M. 2-^{18}F-fluoropropionic acid as a pet imaging agent for prostate cancer. *J. Nucl. Med.* **2009,** *50*, (10), 1709-1714.

47. Dearling, J. L. J.; Lewis, J. S.; Mullen, G. E. D.; Welch, M. J.; Blower, P. J. Copper bis(thiosemicarbazone) complexes as hypoxia imaging agents: structure-activity relationships. *J. Biol. Inorg. Chem.* **2002,** *7*, (3), 249-259.

48. Zhang, Q.; Huang, H.; Chu, T. In vitro and in vivo evaluation of technetium-99m-labeled propylene amine oxime complexes containing nitroimidazole and nitrotriazole groups as hypoxia markers. *J. Labelled Compd. Radiopharm.* **2016,** *59*, (1), 14-23.

49. Li, Z.; Lin, X.; Zhang, J.; Wang, X.; Jin, Z.; Zhang, W.; Zhang, Y. Kit formulation for preparation and biological evaluation of a novel ^{99m}Tc-oxo complex with metronidazole xanthate for imaging tumor hypoxia. *Nucl. Med. Biol.* **2016,** *43*, (2), 165-170.

50. Cao, J.; Liu, Y.; Zhang, L.; Du, F.; Ci, Y.; Zhang, Y.; Xiao, H.; Yao, X.; Shi, S.; Zhu, L.; Kung, H. F.; Qiao, J. Synthesis of novel PEG-modified nitroimidazole derivatives via "hot-click" reaction and their biological evaluation as potential PET imaging agent for tumors. *J. Radioanal. Nucl. Chem.* **2017,** *312*, (2), 263-276.

51. Engelhardt, E. L.; Schneider, R. F.; Seeholzer, S. H.; Stobbe, C. C.; Chapman, J. D. The synthesis and radiolabeling of 2-nitroimidazole derivatives of cyclam and their preclinical evaluation as positive markers of tumor hypoxia. *J. Nucl. Med.* **2002,** *43*, (6), 837-850.

52. Wanek, T.; Kreis, K.; Krizkova, P.; Schweifer, A.; Denk, C.; Stanek, J.; Mairinger, S.; Filip, T.; Sauberer, M.; Edelhofer, P.; Traxl, A.; Muchitsch, V. E.; Mereiter, K.; Hammerschmidt, F.; Cass, C. E.; Damaraju, V. L.; Langer, O.; Kuntner, C. Synthesis and preclinical characterization of 1-(6'-deoxy-6'-[^{18}F]fluoro-β-D-allofuranosyl)-2-nitroimidazole (β-6'-[^{18}F]FAZAL) as a positron emission tomography radiotracer to assess tumor hypoxia. *Bioorg. Med. Chem.* **2016,** *24*, (21), 5326-5339.

53. Lewis, J. S.; McCarthy, D. W.; McCarthy, T. J.; Fujibayashi, Y.; Welch, M. J. Evaluation of ^{64}Cu-ATSM in vitro and in vivo in a hypoxic tumor model. *J. Nucl. Med.* **1999,** *40*, (1), 177-183.

54. Wang, H.; Wu, Z.; Li, S.; Wang, H.; Tang, G.; Hu, K.; Huang, T.; Liang, X. Comparison of three ^{18}F-labeled carboxylic acids with ^{18}F-FDG of the differentiation tumor from inflammation in model mice. *BMC. Med. Imaging.* **2016,** *16*, (1), 1-8.

Table 1. The partition coefficient of [^{18}F]**5** and [^{18}F]**8**, compared with [^{18}F]FMISO. Data were expressed as mean ± SD, n = 3.

Compound	log *P*
[^{18}F]**5**	0.42 ± 0.02
[^{18}F]**8**	0.63 ± 0.03
[^{18}F]FMISO	0.38 ± 0.08

Table 2. Percentages of unchanged radiotracers after incubation in rat blood in vitro. Changes of radiotracers were measured by Radio-HPLC. Data were expressed as mean ± SD, n = 3.

Radiotrsacer	Percentage of unchanged radiotracer (%)		
	2 min	5 min	10 min
[^{18}F]**5**	9.42 ± 0.12	0.41 ± 0.12	0
[^{18}F]**8**	15.23 ± 0.96	3.33 ± 0.80	1.84 ± 0.46

Table 3A Biodistribution of [^{18}F]**5**, [^{18}F]**8**, [^{18}F]FMISO and 2-[^{18}F]FPA in EMT-6 tumor-bearing mice at 30 min after tail vein injection. (%ID/g; mean ± S.D. n = 5)

	30 min			
Tissue	[^{18}F]**5**	[^{18}F]**8**	[^{18}F]FMISO	2-[^{18}F]FPA
Blood	9.45 ± 0.30	8.37 ± 0.75	4.60 ± 0.61	8.29 ± 0.69
Brain	4.85 ± 0.34	5.68 ± 0.33	4.34 ± 0.51	5.98 ± 0.55
Heart	8.10 ± 0.23	9.31 ± 0.77	6.35 ± 0.96	8.64 ± 1.54
Liver	6.95 ± 0.42	6.66 ± 0.52	7.31 ± 0.76	5.98 ± 0.73
Lung	6.99 ± 0.62	7.67 ± 0.43	6.85 ± 0.44	5.47 ± 0.21
Spleen	5.68 ± 0.37	6.18 ± 0.27	4.55 ± 0.59	5.64 ± 0.71
Kidneys	5.21 ± 0.31	5.32 ± 0.20	7.36 ± 0.45	4.87 ± 0.65
Stomach	5.05 ± 0.15	7.53 ± 0.55	5.66 ± 0.90	6.07 ± 1.27
Bone	3.58 ± 0.42	4.95 ± 0.61	3.33 ± 0.70	3.25 ± 0.27
Muscle	5.30 ± 0.27	6.41 ± 0.55	4.53 ± 0.54	6.13 ± 1.47
Skin	3.12 ± 0.24	5.13 ± 0.73	4.44 ± 0.83	5.10 ± 0.52
Tumor	**8.49 ± 0.72**	**8.71 ± 0.81**	**4.41 ± 0.83**	**8.61 ± 0.33**
Tumor-to-liver	1.18 ± 0.08	1.31 ± 0.09	0.63 ± 0.05	1.59 ± 0.02
Tumor-to-muscle	1.55± 0.16	1.38 ± 0.26	1.01 ± 0.14	1.40 ± 0.13

Tumor-to-blood	0.90 ± 0.07	1.04 ± 0.06	0.98 ± 0.03	1.06 ± 0.04

Table 3B Biodistribution of [^{18}F]**5**, [^{18}F]**8**, [^{18}F]FMISO and 2-[^{18}F]FPA in EMT-6 tumor-bearing mice at 60 min after tail vein injection. (%ID/g; mean ± S.D. n = 5)

	60 min			
Tissue	[^{18}F]**5**	[^{18}F]**8**	[^{18}F]FMISO	2-[^{18}F]FPA
Blood	8.69 ± 0.72	8.18 ± 0.77	3.46 ± 0.22	7.95 ± 0.78
Brain	6.09 ± 0.45	6.09 ± 0.43	3.79 ± 0.26	5.63 ± 0.53
Heart	8.61 ± 0.87	8.29 ± 0.71	5.61 ± 0.59	8.42 ± 1.09
Liver	6.57 ± 0.32	6.14 ± 0.65	7.92 ± 0.54	5.71 ± 0.14
Lung	7.29± 0.48	7.41 ± 0.51	5.95 ± 0.34	7.30 ± 0.83
Spleen	6.17 ± 0.21	5.90 ± 0.69	3.60 ± 0.25	5.67 ± 0.48
Kidneys	5.55 ± 0.26	5.01 ± 0.51	6.20 ± 0.44	5.11 ± 0.56
Stomach	6.03 ± 0.38	5.71 ± 0.51	5.31 ± 0.43	5.71 ± 0.37
Bone	5.54 ± 0.91	6.40 ± 0.81	4.51 ± 0.75	4.70 ± 0.65
Muscle	5.84 ± 0.38	6.07 ± 0.59	3.80 ± 0.73	7.13 ± 0.92
Skin	4.14 ± 0.43	5.01 ± 0.69	3.70 ± 0.26	5.37 ± 1.03
Tumor	**8.89 ± 0.42**	**9.03 ± 1.21**	**5.43 ± 0.62**	**8.52 ±0.51**
Tumor-to-liver	1.35 ± 0.09	1.47 ± 0.14	0.69 ± 0.11	1.49 ± 0.06
Tumor-to-muscle	1.47 ± 0.18	1.49 ± 0.18	1.50 ± 0.48	1.27 ± 0.22
Tumor-to-blood	1.03 ± 0.10	1.10 ± 0.07	1.58 ± 0.28	1.12 ± 0.04

Table 3C Biodistribution of [^{18}F]**5**, [^{18}F]**8**, [^{18}F]FMISO and 2-[^{18}F]FPA in EMT-6 tumor-bearing mice at 120 min after tail vein injection. (%ID/g; mean ± S.D. * n = 5, ** n = 3)

	120 min			
Tissue	[^{18}F]**5***	[^{18}F]**8***	[^{18}F]FMISO**	2-[^{18}F]FPA*
Blood	8.55 ± 0.45	7.76 ± 0.75	1.13 ± 0.35	7.67 ± 0.67
Brain	7.46 ± 0.29	5.92 ± 0.72	1.33 ± 0.49	5.30 ± 0.61
Heart	8.59 ± 0.82	8.33 ± 1.32	2.26 ± 0.76	7.68 ± 0.65
Liver	6.59 ±0.37	6.12 ± 0.92	3.85 ± 1.25	5.26 ± 0.14
Lung	7.89 ± 0.55	7.52 ± 0.81	2.38 ± 0.84	7.34 ± 0.57
Spleen	6.33 ± 0.41	6.03 ± 0.90	1.28 ± 0.49	5.43 ± 0.38
Kidneys	5.30 ± 0.24	4.94 ± 0.68	2.33 ± 0.65	4.92 ±0.49
Stomach	5.20 ± 0.49	6.91 ± 0.36	2.96 ± 0.80	5.25 ± 0.76
Bone	8.08 ± 0.18	9.25 ± 0.68	3.65 ± 1.42	8.68 ± 1.88
Muscle	6.07 ± 0.72	6.11 ± 0.51	2.24 ± 0.72	6.53 ± 0.58
Skin	4.76 ± 0.63	6.24 ± 0.51	2.20 ± 0.85	6.29 ± 0.64

Tumor	**8.69 ± 0.78**	**8.41 ± 0.93**	**3.24 ± 1.58**	**7.95 ± 0.37**
Tumor-to-liver	1.24 ± 0.03	1.37 ± 0.09	0.82 ± 0.12	1.51 ± 0.03
Tumor-to-muscle	1.23 ± 0.21	1.38 ± 0.07	1.45 ± 0.42	1.23 ± 0.14
Tumor-to-blood	1.00 ± 0.05	1.08 ± 0.05	2.79 ± 0.43	1.08 ± 0.02

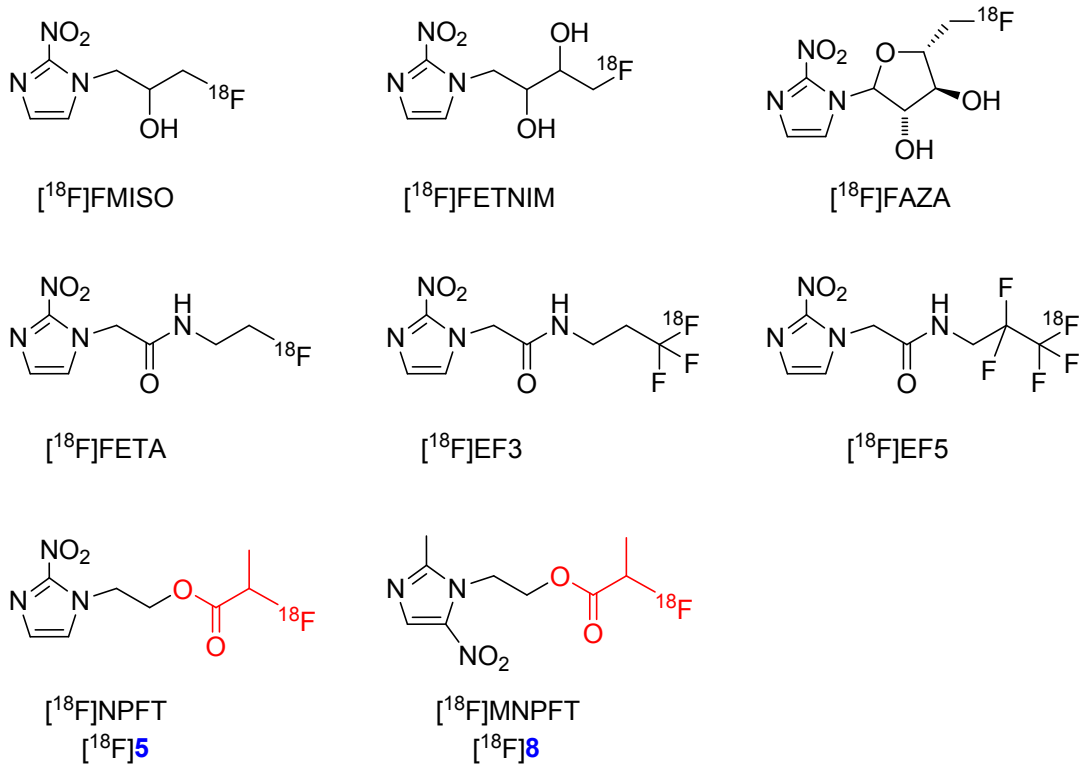

Figure 1. Various ^{18}F-labeled PET-tracers based on nitroimidazole structure.

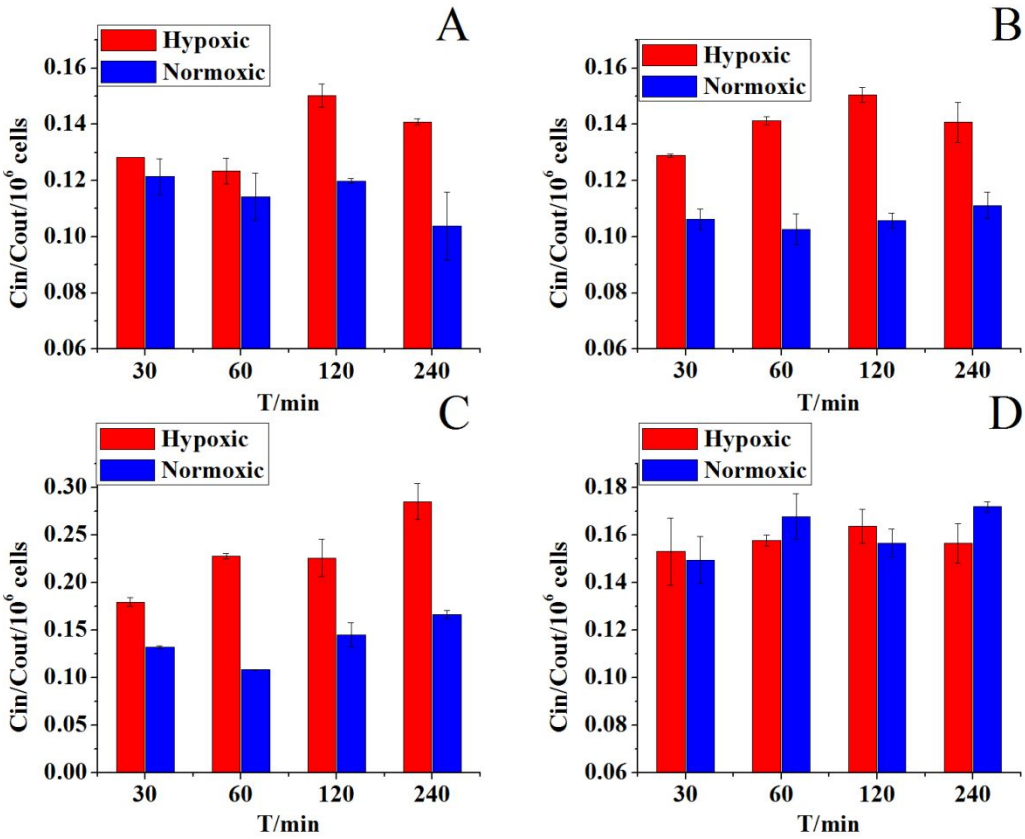

Figure 2. In vitro cell uptake (EMT-6 tumor cells) of [^{18}F]**5*** (A), [^{18}F]**8**** (B), [^{18}F]FMISO** (C) and 2-[^{18}F]FPA*** (D) under hypoxic (5% CO_2 plus 95% N_2) and normoxic (5% CO_2 plus 95% air) conditions after incubation for 30, 60, 120 and 240 min, respectively. Data are expressed as mean ± SD. (n = 3), *P*-values show comparisons of uptake under normoxic and hypoxic conditions (*t*-test): $^{*}P < 0.05$, $^{**}P < 0.01$, $^{***}P > 0.05$. In vitro cell uptake study as expected showed that [^{18}F]**5** (**A**), [^{18}F]**8** (**B**), [^{18}F]FMISO (**C**) displayed highly significant hypoxia selectivity in EMT-6 cell, while 2-[^{18}F]FPA (**D**) showed no difference in cell uptake between nomoxic and hypoxic conditions.

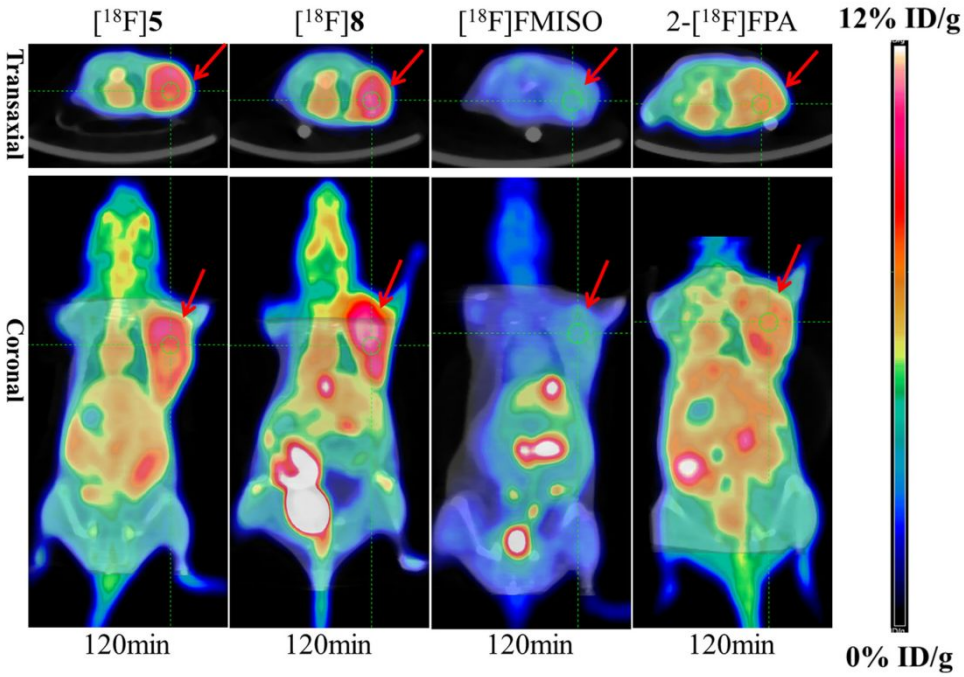

Figure 3. Transaxial and coronal PET/CT fusion images of [^{18}F]**5**, [^{18}F]**8**, [^{18}F]FMISO and 2-[^{18}F]FPA at 120 min post-injection (5.55–11.1 MBq/0.1 mL per mouse via the tail vein) in BALB/c mice bearing EMT-6 tumor. The red arrows represent the location of tumors.

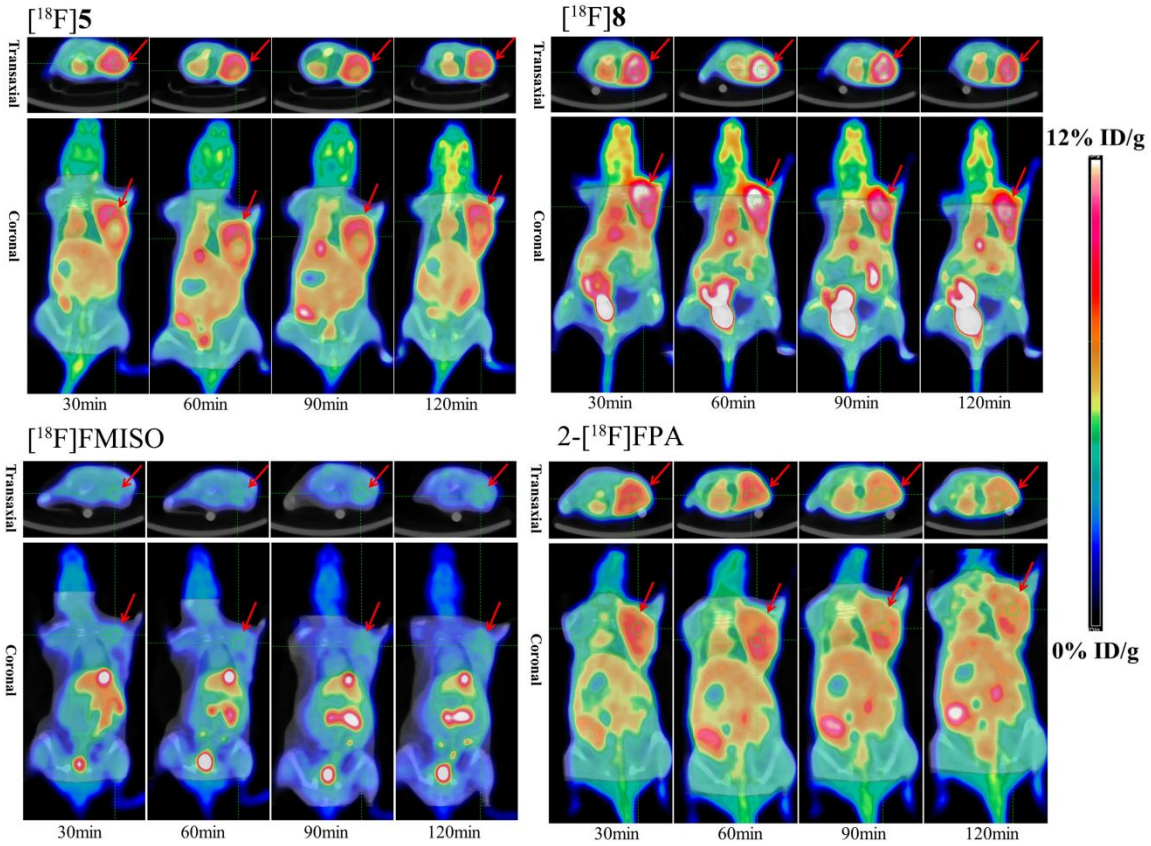

Figure 4. Transaxial and coronal PET/CT fusion images of [^{18}F]**5**, [^{18}F]**8**, [^{18}F]FMISO and 2-[^{18}F]FPA at 30, 60, 90 and 120 min post-injection (5.55–11.1 MBq/0.1 mL per mouse via the tail vein) in BALB/c mice bearing EMT-6 tumor. The red arrows represent the location of tumors.

Scheme 1. Synthesis of radiolabelling precursor 4 and non-radioactive standard [^{19}F]5.

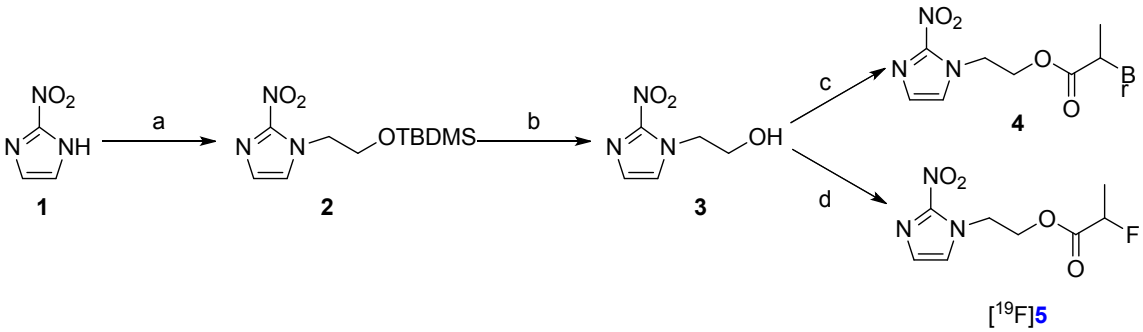

Reagents and conditions: (a) $BrCH_2CH_2OTBDMS$, K_2CO_3, DMF, 100°C, 4 h; (b) 1%HCl-ethanol,

THF, rt, 3 h; (c) $CH_3CHBrCBrO$, Et_3N, DCM, rt, overnight; (d) $FCH(CH_3)COOH$, EDCI, HOBt, DIPEA, DMF, 0°C, 2 h, then rt, overnight.

Scheme 2. Synthesis of radiolabelling precursor 7 and non-radioactive standard [^{19}F]8.

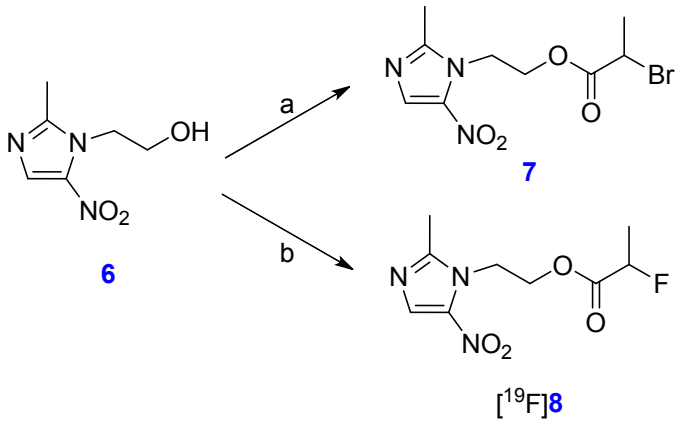

Reagents and conditions: (a) $CH_3CHBrCBrO$, Et_3N, DCM, rt, overnight; (b) $FCH(CH_3)COOH$, EDCI, HOBt, DIPEA, DMF, 0°C, 2 h, then rt, overnight.

Scheme 3. Radiosynthesis of [^{18}F]5 and [^{18}F]8.

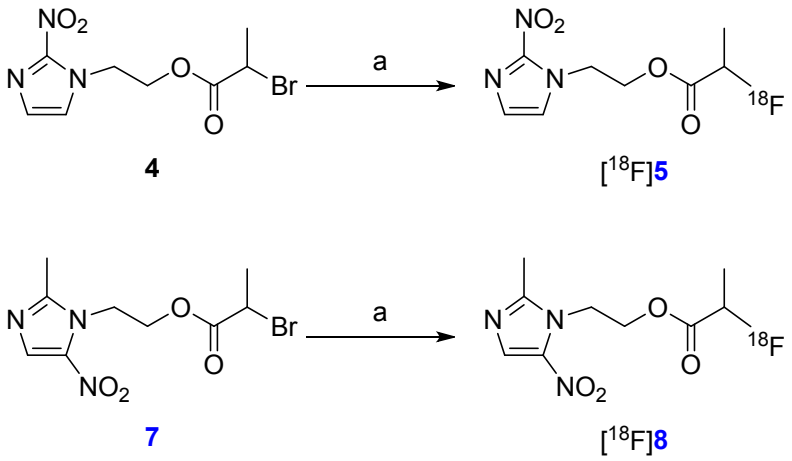

Reagents and conditions: (a) [^{18}F]KF/18-crown-6, $KHCO_3$, acetonitrile, 80°C, 10 min.

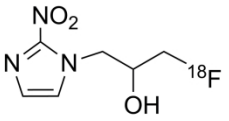

[^{18}F]FMISO

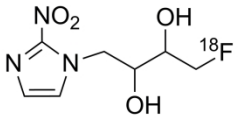

[^{18}F]FETNIM

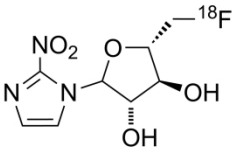

[^{18}F]FAZA

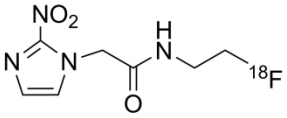

[^{18}F]FETA

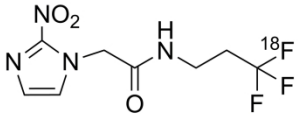

[^{18}F]EF3

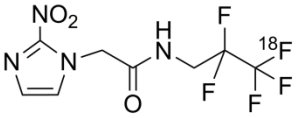

[^{18}F]EF5

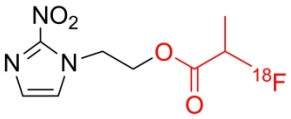

[^{18}F]NPFT
[^{18}F]**5**

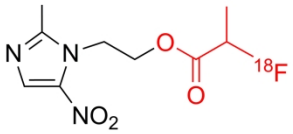

[^{18}F]MNPFT
[^{18}F]**8**

143x102mm (600 x 600 DPI)

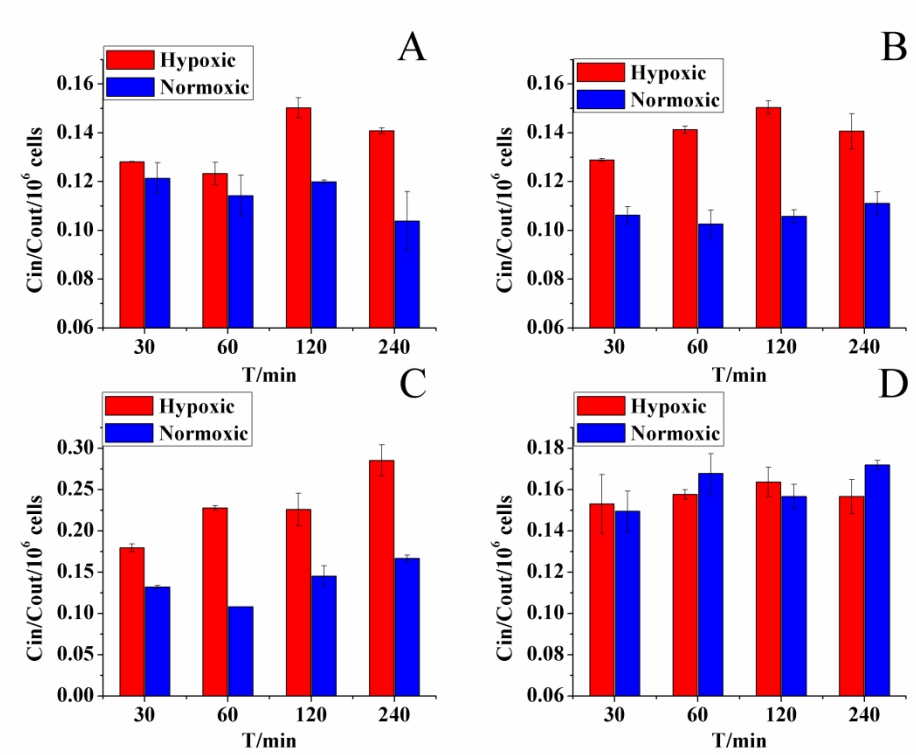

287x220mm (300 x 300 DPI)

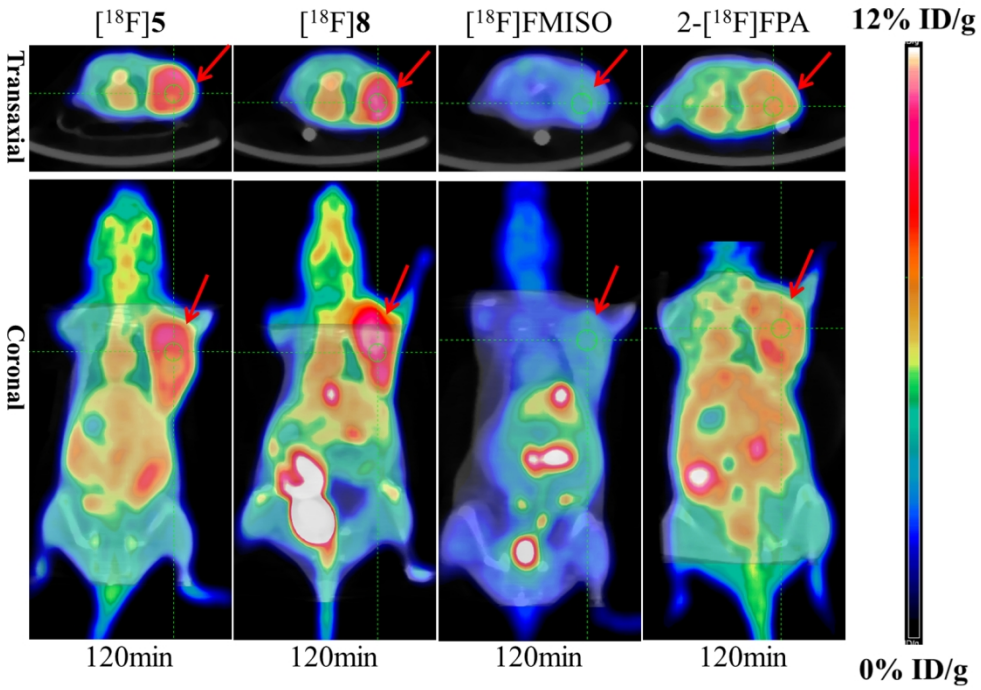

140x99mm (300 x 300 DPI)

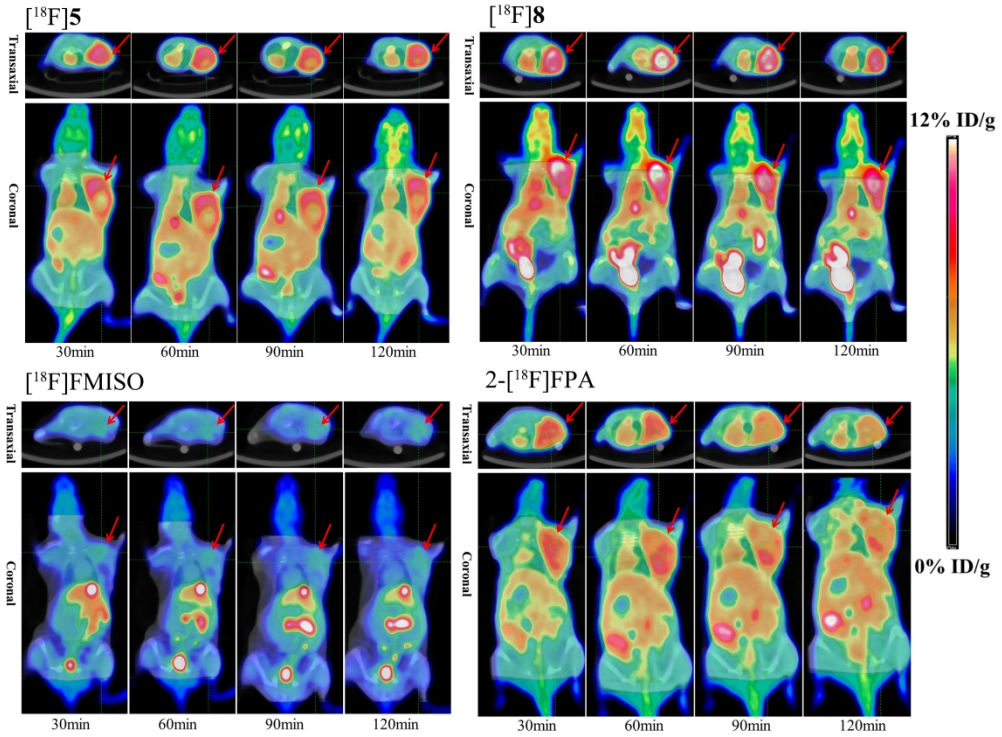

246x183mm (300 x 300 DPI)

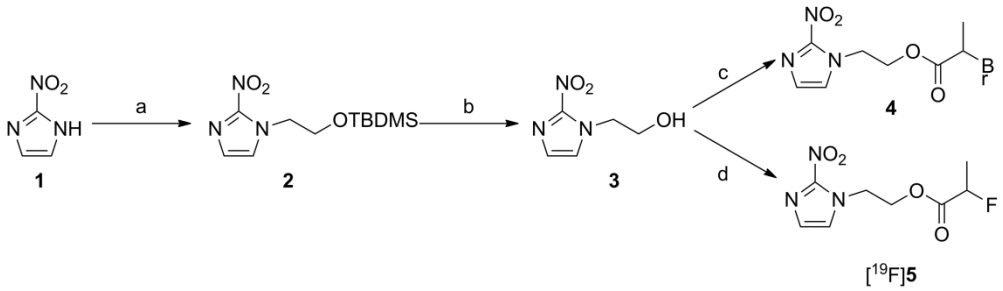

174x50mm (600 x 600 DPI)

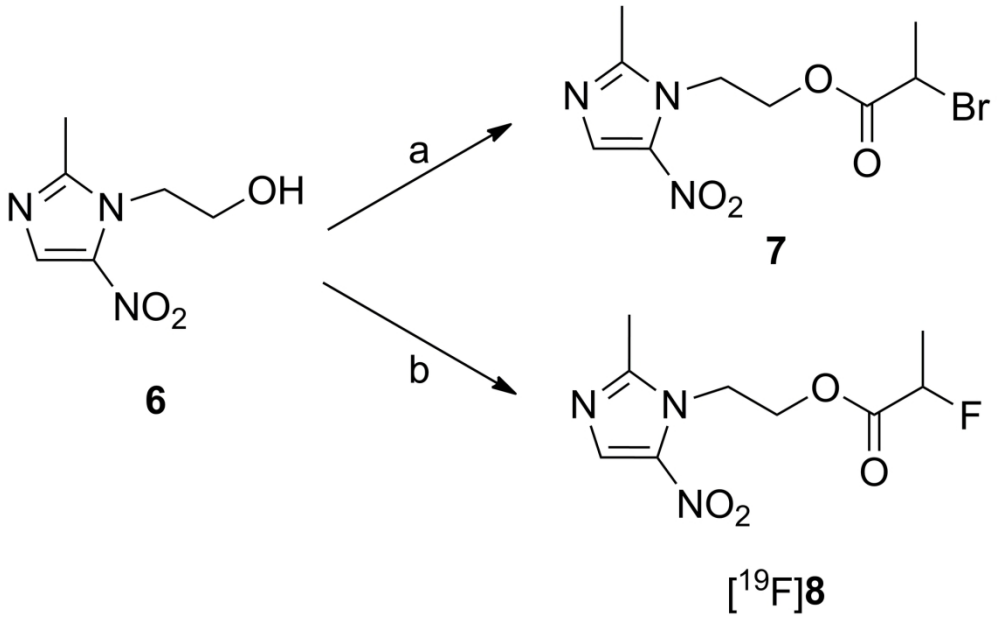

90x56mm (600 x 600 DPI)

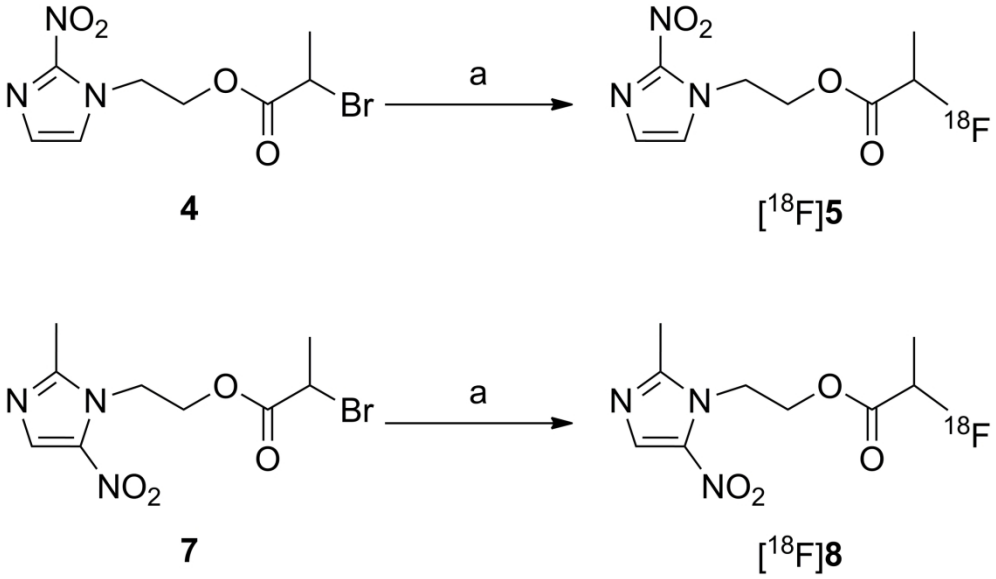

104x61mm (600 x 600 DPI)

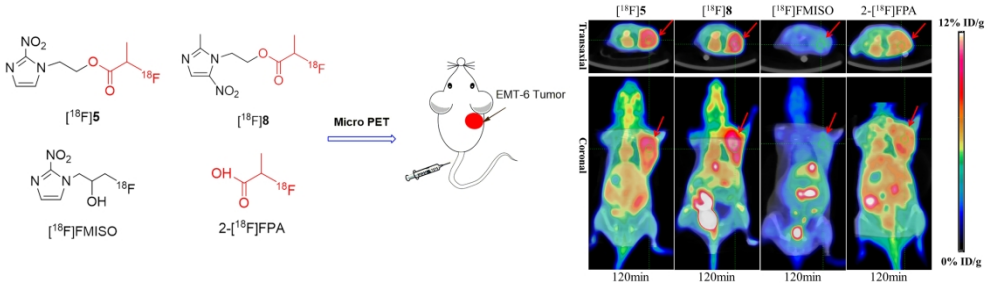

Table of Content Graphic

409x114mm (300 x 300 DPI)